Journal of Infrared, Millimeter, and Terahertz Waves (2020) 41:1355–1365
https://doi.org/10.1007/s10762-020-00670-w

Assignment of Terahertz Modes in Hydroquinone Clathrates

Wei Zhang[1] · Zihui Song[2] · Michael T. Ruggiero[2] · Daniel M. Mittleman[1]

Received: 7 November 2019 / Accepted: 15 January 2020 / Published online: 29 January 2020

Abstract
Hydroquinone (HQ) and its clathrate are materials of growing interests, due to their promising applications in energy related science and industries. Recently, many studies have been performed to understand the properties of these materials. Terahertz (THz) spectroscopy is a powerful tool for studying the properties of these materials by non-destructively probing their low-energy (meV) dynamics. Although terahertz spectra of HQ and its clathrates have been measured, a report on the correspondence between THz spectra and low frequency dynamics is still lacking. In this paper, we measure the temperature-dependent THz spectra of both α-HQ (the non-clathrate form) and β-HQ clathrate, with Ar and CO_2 as guest species. We also perform density functional theory (DFT) simulations on these materials, in order to assign the spectral features. We find an excellent match between the experimental and the DFT calculated spectra. Using the simulation result, we build connections between the THz spectra and the atomic motions in these materials. In addition, we also perform DFT simulations on β-HQ-He, β-HQ-Ne, and β-HQ-Kr to study the patterns in the change of THz spectra as the guest species changes.

Keywords Porous materials · Vibrational spectroscopy · Density functional theory · Lattice dynamics

1 Introduction

Clathrates are a type of inclusion compound in which guest molecules are non-covalently trapped within a framework of a host species. In recent years, hydroquinone (HQ), and its clathrates, have become materials of great interest, due to their potential applications in the

✉ Michael T. Ruggiero
michael.ruggiero@uvm.edu

✉ Daniel M. Mittleman
daniel_mittleman@brown.edu

[1] School of Engineering, Brown University, 184 Hope St, Providence, RI 02912, USA

[2] Department of Chemistry, University of Vermont, 82 University Place, Burlington, VT 05405, USA

energy-related sciences and industries. Hydroquinone is highly selective in the rate of forming clathrates, depending on the guest species, and thus may prove useful in various applications including gas separation, decarbonization, and global warming prevention [1, 2]. Hydroquinone is also a promising hydrogen-storage material [3–5], as well as a platform for studying quantum behaviors of trapped molecules [6, 7].

Various measurement approaches, such as X-ray diffraction, Raman spectroscopy, nuclear magnetic resonance spectroscopy, and neutron diffraction have been applied to understand the properties of HQ and its clathrates [1, 8–10]. Given the importance of weak and non-covalent intermolecular forces for the formation and properties of HQ clathrates, there is a need for experiments that can effectively probe these phenomena. Terahertz time-domain spectroscopy (THz-TDS), a measurement approach that is extremely useful in characterizing the low-frequency dynamics of materials [11–15], has also been used in the measurements of HQ and its clathrates [1, 16, 17]. However, a detailed description of the atomic-level dynamics and associated energetic forces is still lacking.

In this paper, we measure the temperature-dependent THz spectra of both α-HQ (the non-clathrate form) and β-HQ clathrate, with Ar and CO_2 as guest species. We also perform solid-state density functional theory (DFT) simulations on these materials, in order to assign the spectra. We find an excellent match between the experimental and the DFT calculated spectra. Using the simulation result, we build connections between the THz spectra and the atomic motions in these materials. In addition, we also perform DFT simulations on β-HQ-He, β-HQ-Ne and β-HQ-Kr, to study the patterns in the change of THz spectra as guest species changes, ultimately uncovering the nature of the intermolecular forces present in this exciting class of materials.

2 Methods

2.1 Experimental Setup

α-HQ (≥ 99.5%) was purchased from Sigma-Aldrich without any processing. β-HQ-CO_2 is formed by mixing α-HQ and pressurized CO_2 (850 psi, 99.99%) at 303 K for two weeks. β-HQ-Ar was formed by mixing α-HQ and pressurized Ar (5000 psi, 99.999%) at 333 K for two months. Furthermore, a common way of generating gas-HQ clathrates is to pressurize the gas and HQ mixture under room temperature over time [10, 18]. However, we use a slightly higher temperature (higher than room T but lower than the decomposition T) to accelerate the reaction. As for the reaction time, we continuously measure the sample's THz spectrum to monitor the reaction progress and stop the reaction when most of the samples are reacted (which takes about 2 months). The samples were pressed into thin sample tablets using approximately 0.1 GPa of pressure, to produce pellets with a thickness of around 0.2 mm and a diameter of 6 mm. These tablets were then attached to thick polyethylene spacers with a thickness of around 2.3 mm and the same diameter. These sample tablets are placed into a cryostat for temperature-dependent THz time-domain spectroscopy (THz-TDS) measurements. The experimental configuration is reported in reference [19].

2.2 Simulation Settings

Solid-state DFT simulations were performed using the fully-periodic CRYSTAL17 software package [20]. The generalized gradient approximation (GGA) Perdew-Burke-Ernzerhof (PBE)

density functional was used [21]. London dispersion forces were accounted for using the Grimme DFT-D3 correction, with the Becke-Johnson damping function and including many-body dispersion corrections, which are important for accurately modeling the van der Waals forces that drive the guest-host interactions [22]. The electrons were represented with the Ahlrichs valence triple-ζ and polarization (VTZP) basis set for all calculations [23]. Reciprocal space sampling was performed using the Monkhorst–Pack scheme, with a $6 \times 6 \times 6$ k-point mesh in the 1st Brillouin Zone (program keyword SHRINK: 6 6), corresponding to a total of 40 points for both α-HQ and β-HQ, once Bravais symmetry was taken into account. The tolerances for Coulomb and exchange integral cutoffs were set to $\Delta E < 10^{-8}$ E_h (program keyword TOLINTEG: 8 8 8 8 16). All structures underwent geometry optimization, and the calculations were initiated using the experimental atomic positions and lattice vectors retrieved from Cambridge Crystallographic Data Centre (CCDC) database [18, 24, 25]. All atoms and lattice vectors were allowed to fully relax within the space group symmetry of the solid. The energy convergence criterion was set to $\Delta E < 10^{-8}$ E_h (program keyword TOLDEE: 8) Then, frequency calculations were executed by using the optimized coordinates and lattice parameters to yield the vibrational modes and IR intensities. Eigenvalues and eigenvectors were calculated numerically through harmonic approximation, which has previously proven effective for vibrational normal modes [26, 27], and IR intensities were calculated using the Berry phase method [28, 29]. The energy convergence criterion was set to a more stringent value from the geometry optimization, $\Delta E < 10^{-11}$ E_h. Because it is well-known that vibrational line shapes generally follow Lorentzian behavior, the simulated vibrational spectra were generated using a sum of Lorentzian functions with empirically determined linewidths. In the case of β-HQ-CO_2, a very recently developed anharmonic correction was utilized to reveal the fundamental transition frequency using the vibrational self-consistent field method [30, 31]. A potential energy scan along the identified normal mode was generated, followed by fitting with a 6th order polynomial, and the anharmonic oscillator Schrodinger equation was solved.

3 . Results and Discussion

3.1 Structural Analysis

α-HQ (CSD reference code: HYQUIN02) forms a rhombohedral crystal with a space group of $R\bar{3}$ as revealed by X-ray diffraction studies [32], and the structure is shown in Fig. 1a. α-HQ contains 54 molecules in the unit cell with 3 symmetry-independent molecules in the crystal structure. Its lattice parameters are $a = b = 38.46$ Å, $c = 5.650$ Å, $\alpha = \beta = 90°$, and $\gamma = 120°$. The structure consists of an infinite hydrogen bonding network of HQ molecules, with each molecule accepting and donating two hydrogen bonds, respectively. The unit cell contains two porous sites, with a stoichiometry corresponding to a ratio of 1 site per 18 HQ molecules. The α-form is not considered to be the clathrate forming compound because of the limited number of binding sites in the solid. The unit cell structure shown in Fig. 1a. A good match is found between the simulation and the experimental results, with an average error in lattice parameters between the experimental and predicted geometries of 0.40%.

In contrast, the β-form of HQ (CSD reference code: HYQUIN08) is a repeated network of clathrate cages, with the unit cell shown in Fig. 1b. It has the same space group as the α-form, $R\bar{3}$, but it contains only 9 molecules in the unit cell, with the symmetry unique unit of only half

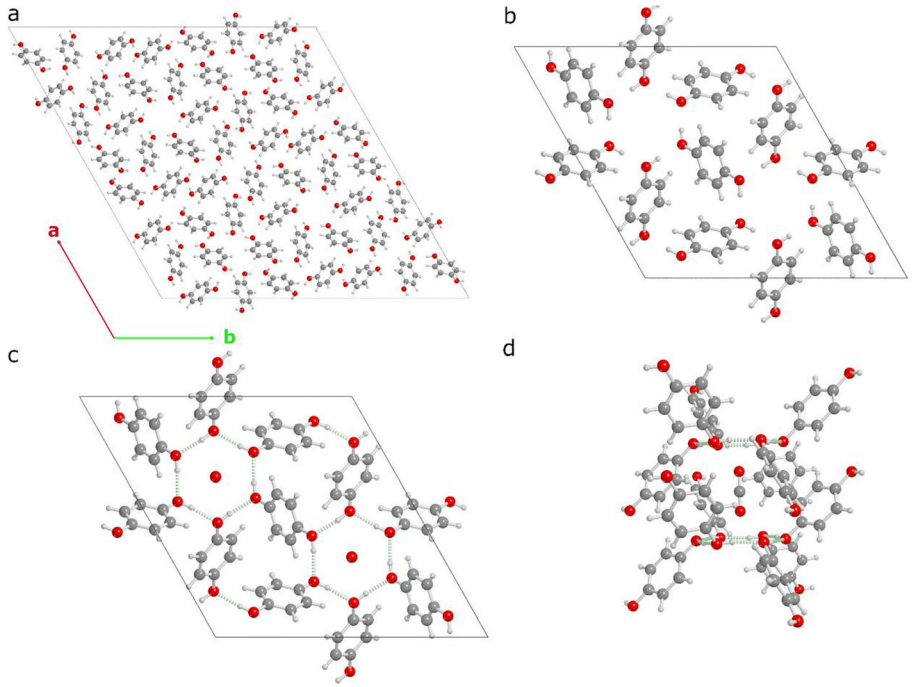

Fig. 1 The structures of hydroquinone crystals investigated. **a** The unit cell of α-HQ; **b** the unit cell of β-HQ; **c** the unit cell of β-HQ-CO_2; and **d** an extracted clathrate cage, showing the CO_2 guest in a cavity formed by two adjacent hydrogen bonding planes, highlighting the weak interactions that the guest molecules experience

of a molecule. It has unit cell parameters of $a = b = 16.59$ Å, $c = 5.45$ Å, $\alpha = \beta = 90°$, and $\gamma = 120°$. The β-HQ is the clathrate forming polymorph since there are abundant binding sites in the solid, with a porous site to HQ molecule stoichiometry of 1:3. Figure 1c shows the structure of the system when a guest molecule is present, in this case CO_2 (β-HQ-CO_2),

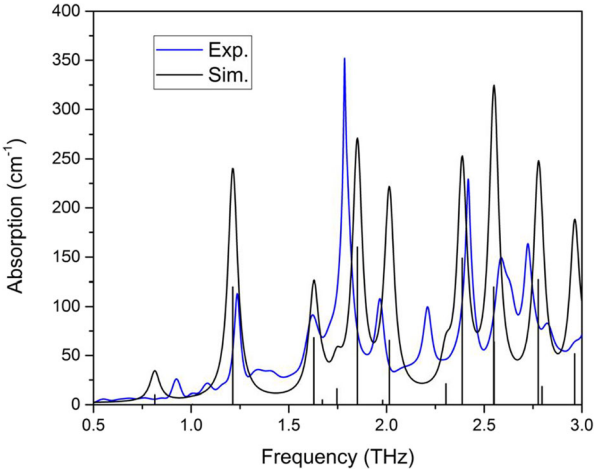

Fig. 2 Experimental (blue) and DFT simulated (black) THz spectra of α-HQ. The experimental data is measured at 120 K. The black vertical bars indicate the eigen modes of α-HQ calculated by DFT simulation

Table 1 THz mode frequencies, intensities, and primary mode types of α-HQ

Frequency (THz)	Intensity (km mol^{-1})	Description
0.814	1.24	External rotation around cage center
1.007	0.05	External rotation around cage center
1.213	9.52	HQ rotation around its principle axis
1.628	4.52	Coupled symmetric rotation around principle axis
1.672	0.61	Coupled symmetric rotation around principle axis
1.746	0.99	Coupled anti-symmetric rotation around principle axis
1.849	20.56	Anti-symmetric rotation of HQ about principle axis
1.979	0.56	Anti-symmetric translation
2.013	8.18	Anti-symmetric translation
2.302	1.32	Coupled symmetric rotation
2.386	18.61	Coupled antisymmetric rotation
2.547	8.66	Antisymmetric rotation of non-cage forming HQ
2.549	7.99	Rotation perpendicular to HQ ring
2.775	8.41	Antisymmetric rotation
2.794	2.28	Antisymmetric translation
2.961	6.46	Antisymmetric rotation

which is similar to all of the β-HQ-X structures studied here as well as the empty β-HQ solid. As shown in Fig. 1d, the guest sits in a site that is adjacent to two hydrogen bonded rings, with no directed interactions pointing into the pore.

3.2 Terahertz Time-Domain Spectroscopy

The dynamics of the HQ systems were probed using THz-TDS. The experimental and simulated spectra for α-HQ are shown in Fig. 2, with the simulated mode frequencies, intensities, and assignments (representing the major motions present) presented in Table 1. There are a relatively large number of phonon modes in α-HQ below 3 THz, caused by the fact that its unit cell contains a large number of atoms. The modes are primarily external coupled

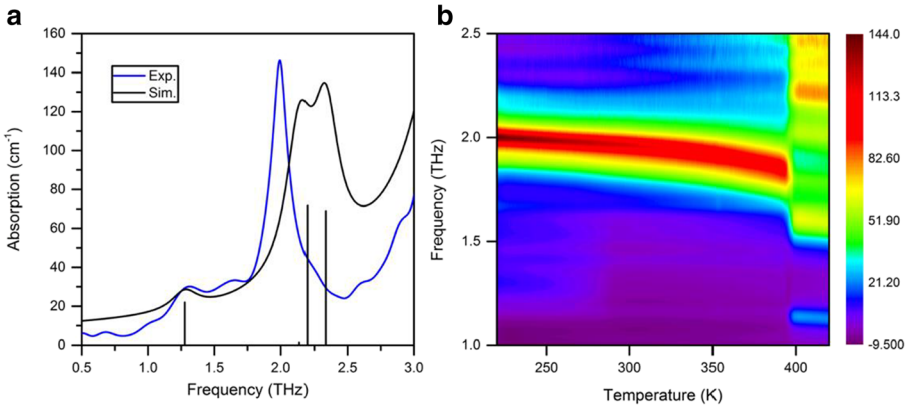

Fig. 3 **a** Experimental (blue) and DFT simulated (black) THz spectra of β-HQ-Ar. The experimental data is measured at 220 K. The black vertical bars indicate the eigen modes of β-HQ-Ar calculated by DFT simulation. **b** Temperature-dependent experimental THz spectra of β-HQ-Ar. The major mode near 2 THz red-shifts as temperature increases. Near 395 K, the sample's spectrum drastically changes, corresponding to the phase transition from β-HQ to α-HQ, accompanied by releasing the guest molecules (Ar)

Table 2 THz Mode frequencies, intensities, and motion descriptions of β-HQ-Ar

Frequency (THz)	Intensity (km mol^{-1})	Description
1.2763	0.19	Ar translation in the *b*-*c* plane
1.4310	0.06	Ar translation in the *a*-*c* plane
2.1370	1.39	HQ anti-symmetric translational motion perpendicular to the *a*-*c* plane
2.3334	2.95	HQ anti-symmetric translational motion in the *a*-*c* plane

motions of the HQ-molecules, consisting of a combination of symmetric and anti-symmetric rotations and translations.

We perform similar analysis on β-HQ-Ar, with the spectra shown in Fig. 3 and the mode details shown in Table 2. Comparing with the experimental result, the simulation predicts two significant modes near 2 THz, while the experimental data only shows a single peak at the same frequency. Based on inspection of the experimental spectrum, it can be observed that the major feature at ~2 THz is significantly broader than in our other presented spectra collected at the same temperature, with a FWHM of 0.22 THz, compared with an average FWHM of 0.08 for β-HQ-CO_2 at the same temperature. This indicates that this feature likely is a sum of two closely space discrete transitions, in line with the theoretical simulations. We also measured the temperature-induced decomposition of β-HQ-Ar, as shown in Fig. 3b. Near 395 K, the sample's spectrum drastically changes, corresponding to the phase transition from β-HQ to α-HQ, accompanied by the release of guest molecules (Ar).

Our experimental (123 K) and DFT simulated THz spectra of β-HQ-CO_2 are shown in Fig. 4a**.** The initial simulation results, while generally in agreement with the experimental spectrum, has an obvious disagreement for the third absorption feature, which is underestimated in frequency compared with the experimental peak. The temperature dependent THz-TDS experiments highlight that this particular feature shifts considerably more with temperature compared with the others, indicating it is likely very anharmonic. Indeed, a potential energy scan of the three modes confirm this, with the first two modes following harmonic behavior,

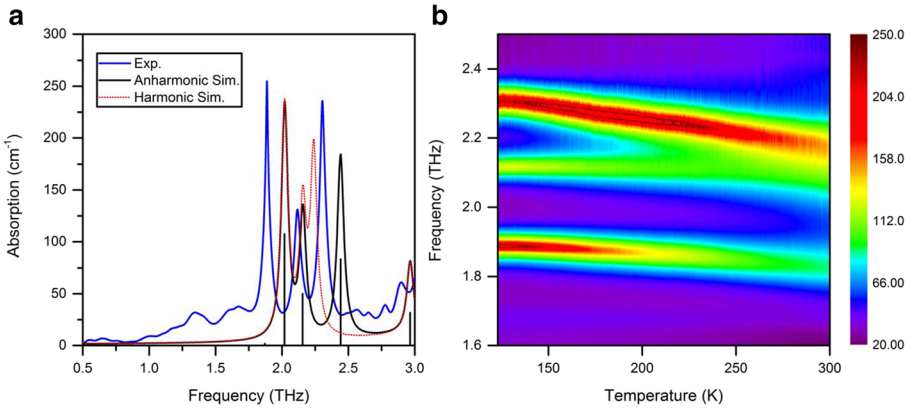

Fig. 4 **a** Experimental (blue) and the harmonic and anharmonic DFT simulated (dotted red and black, respectively) THz spectra of β-HQ-CO_2. The experimental data is measured at 123 K. The black vertical bars indicate the eigen modes of β-HQ-CO_2 calculated by anharmonic-corrected DFT simulation. **b** Temperature-dependent experimental THz spectra of β-HQ-CO_2. The 3rd mode blue-shifts significantly as temperature increases, while the frequency of the 1st and 2nd modes shift to a much lesser extent. At room temperature, the 2nd and 3rd modes overlap, thus only two major THz modes can be observed below 3 THz

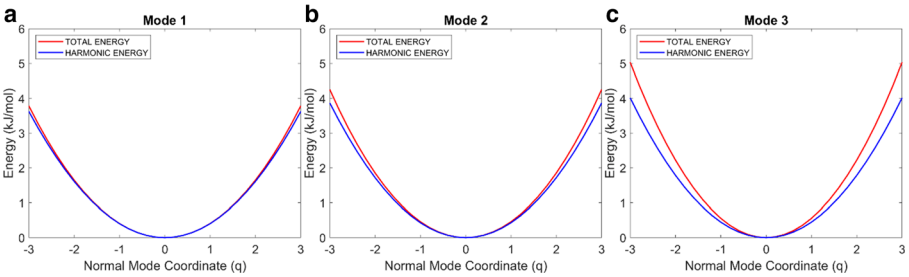

Fig. 5 Potential energy scans for the three observed modes in β-HQ-CO2. Mode 1 and 2 exhibit only minor deviations compared with harmonic behavior, while Mode 3 clearly deviates significantly, even at small displacements

while the third mode deviates significantly, as shown in Fig. 5. Therefore, we have utilized a recently developed vibrational algorithm [30, 31] to determine the anharmonic vibrational frequency for the mode, which resulted in a transition frequency of 2.44 THz, in much better agreement with the experimental spectrum.

As shown in Fig. 4, an excellent match is found between the simulation and the experimental results. Table 3 lists the THz mode frequencies, intensities and motion descriptions of β-HQ-CO_2. β-HQ-CO_2 has 3 major phonon modes below 3 THz: the first two modes correspond to CO_2 translational motions in a rigid cage (cage rattling), while the third mode corresponds to the motion of the cage itself. Figure 5b illustrates the temperature-dependent experimental THz spectra of β-HQ-CO_2. At room temperature, the 2nd and 3rd modes overlap, thus only two major THz modes can be observed below 3 THz.

To understand the impact of guest molecules on the THz modes, we compare the DFT simulation results of β-HQ-X, where X = He, Ne, Ar, and Kr (Fig. 6). These materials, because they have nearly identical crystal structures, represent a rare case where peak shifting between different samples can be interpreted quantitatively, as we have previously shown [33]. All four materials have very similar spectra near 2 THz, caused by the fact that the modes near 2 THz are primarily cage modes, which have little dependence on the species of guest molecules. However, the peak at lower frequency significantly depends on the guest species (~0.4 THz for X = He, ~0.6 THz for X = Ne, ~1.2 THz for X = Ar, ~1.1 THz for X = Kr), due to the fact that this peak corresponds to the cage-rattling modes (translational motions of guest molecules), and thus is susceptible to the properties (e.g. weight and size) of the guest species. As shown in Table 4, the force constant and reduced masses of the various solids were determined. While the increasing mass should result in a decrease in vibrational frequency, the results show that there is a simultaneous increase in force constant with increasing mass, leading to the observed results.

Table 3 THz mode frequencies, intensities, and motion descriptions of β-HQ-CO_2

Frequency (THz)	Intensity (km mol^{-1})	Description
2.0188	2.15	CO_2 translation along *b*-*c* plane
2.1556	1.14	CO_2 translation in *b*-*c* plane
2.2373	3.35	HQ antisymmetric rotation
2.9629	1.27	CO_2 translation in *a*-*b* plane

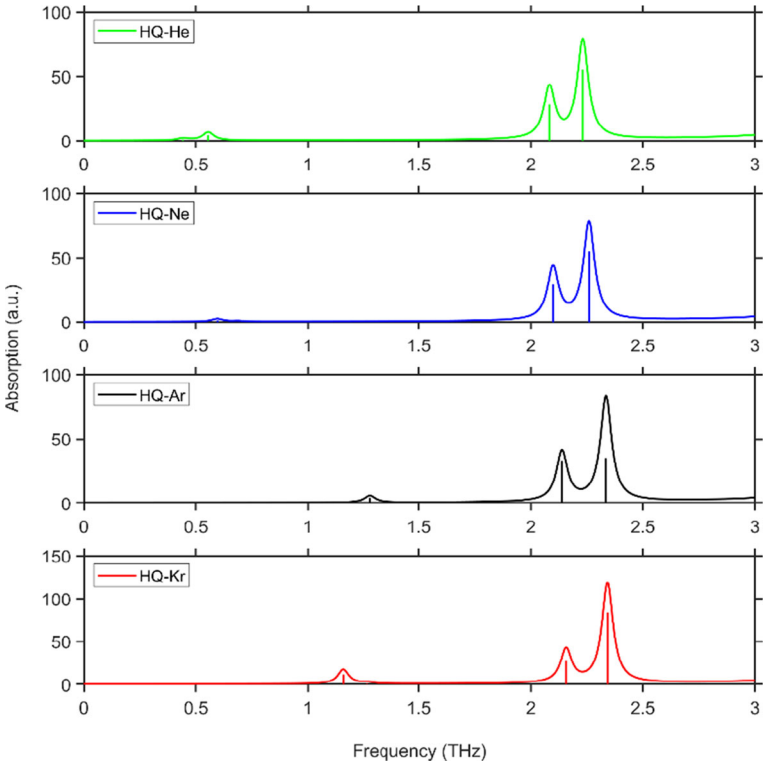

Fig. 6 Simulated vibrational spectra of β-HQ-X, where X = He (green), Ne (blue), Ar (black), and Kr (red). The cage-rattling mode frequency differs for different guest species, while the frequencies of the cage modes almost remain constant

3.3 Energetic Analysis

Given that the increasing force constant likely is due to dispersion forces, the binding energies of these materials were predicted. The energies were decomposed into the binding energy of the gas molecules within the cage, by the following formula:

$$E_{Binding} = E_{UC} - \left(E_{Empty} + E_{Gas}\right)$$

where E_{UC} is the energy of the HQ + X crystal, E_{Empty} is the energy of the empty framework, and E_{Gas} is the energy of the isolated gas molecule. It is important to note that all of the calculated energies have been corrected for basis set superposition error (BSSE) using the

Table 4 Cage-rattling vibrational frequency, reduced mass (Dalton, Da), and force constant (N/m) in noble gas HQ clathrates

β-HQ-X	Frequency (THz)	Reduced mass (Da)	Force constant (N/m)
He	0.44	4.03	0.05
Ne	0.59	18.36	0.427
Ar	1.28	27.00	2.886
Kr	1.16	27.74	2.439

Table 5 The binding energy between the HQ framework and guest gas molecule, the dispersion contribution to the binding energy, and the ratio of the dispersion energy to the total binding energy

β-HQ-X	Binding energy (kJ/mol)	Dispersion contribution to binding energy (kJ/mol)	Ratio of dispersion energy to the total binding energy (%)
He	−6.78	−3.69	54.35
Ne	−13.81	−6.13	44.43
Ar	−26.40	−23.38	88.57
Kr	−43.02	−32.64	75.88
CO_2	−44.36	−38.22	86.17

counterpoise method [34]. The results are shown in the Table 5. For β-HQ-X (X=He, Ne, Ar, Kr), the overall binding energy is increased with increasing the atomic mass. However, when the energy is decomposed further, by determining the dispersion energy contribution, a surprising trend emerges, notably for the β-HQ-Kr material. The results show that while the dispersion energy increases with increasing mass, as expected, the relative contribution of the dispersion energy to the total energy decreases when moving from β-HQ-Ar to β-HQ-Kr. This signifies that the relative binding energies are non-linear, and likely (in the case of β-HQ-Kr) other forces, such as induced-dipole forces, play a competing role. Moreover, these results help to shed light on the non-linear peak shifting observed in the simulated terahertz spectra, as with β-HQ-Kr, its large size likely results in an overall weaker interaction with the β-HQ framework, resulting in the observed decreased force constant.

4 Conclusions

We measure the temperature-dependent THz spectra of both α-HQ (the non-clathrate form) and β-HQ clathrate, with Ar and CO_2 as guest species, and assign the measured spectral features to atomic motions using DFT simulations. We also perform DFT simulations on β-HQ-Ne and β-HQ-Kr to study the patterns in the change of THz spectra as guest species changes. Our results build direct connections between the low-energy (phonon) dynamics and the THz spectra of HQ and its clathrates, paving the way for further studies on the properties of these materials.

References

1. Y. J. Lee, K. W. Han, J. S. Jang, T. I. Jeon, J. Park, T. Kawamura, Y. Yamamoto, T. Sugahara, T. Vogt, J. W. Lee, Y. Lee, and J. H. Yoon, "Selective CO_2 trapping in guest-free hydroquinone clathrate prepared by gas-phase synthesis," *ChemPhysChem,* **12**, 1056–1059, 2011.
2. R. Coupan, C. Dicharry, and J. P. Torré, "Hydroquinone clathrate based gas separation (HCBGS): Application to the CO_2/CH_4 gas mixture," *Fuel,* **226**, 137–147, 2018.
3. J. L. Daschbach, T. M. Chang, L. R. Corrales, L. X. Dang, and P. McGrail, "Molecular mechanisms of hydrogen-loaded beta-hydroquinone clathrate," *J. Phys. Chem. B,* **110**, 17291–17295, 2006.
4. A. W. van den Berg and C. O. Arean, "Materials for hydrogen storage: current research trends and perspectives," *Chem. Commun.,* **14**, 668–681, 2008.
5. K. W. Han, Y. J. Lee, J. S. Jang, T. I. Jeon, J. Park, T. Kawamura, Y. Yamamoto, T. Sugahara, T. Vogt, J. W. Lee, Y. Lee, and J. H. Yoon, "Fast and reversible hydrogen storage in channel cages of hydroquinone clathrate," *Chem. Phys. Lett.,* **546**, 120–124, 2012.
6. S. Takeda, H. Kataoka, K. Shibata, S. Ikeda, T. Matsuo, and C. J. Carlile, "Quantum precession of HCl molecule in hydroquinone clathrate," *Physica B,* **202**, 315–319, 1994.

7. T. A. Strobel, A. J. Ramirez-Cuesta, L. L. Daemen, V. S. Bhadram, T. A. Jenkins, C. M. Brown, and Y. Q. Cheng, "Quantum dynamics of H_2 trapped within organic clathrate cages," *Phys. Rev. Lett.,* **120**, 120402, 2018.
8. J. C. A. Boeyens and J. A. Pretorius, "X-ray and neutron diffraction studies of the hydroquinone clathrate of hydrogen chloride," *Acta Cryst. B,* **33**, 2120–2124, 1977.
9. J. W. Lee, K. J. Choi, Y. Lee, and J. H. Yoon, "Spectroscopic identification and conversion rate of gaseous guest-loaded hydroquinone clathrates," *Chem. Phys. Lett.,* **528**, 34–38, 2012.
10. R. Coupan, E. Pere, C. Dicharry, and J. P. Torré, "New insights on gas hydroquinone clathrates using *in situ* Raman spectroscopy: Formation/dissociation mechanisms, kinetics, and capture selectivity," *J. Phys. Chem. A,* **121**, 5450–5458, 2017.
11. J. E. Pedersen and S. R. Keiding, "THz time-domain spectroscopy of nonpolar liquids," *IEEE J. Quant. Elec.,* **28**, 2518–2522, 1992.
12. M. T. Ruggiero, J. Sibik, R. Orlando, J. A. Zeitler, and T. M. Korter, "Measuring the elasticity of poly-L-proline helices with terahertz spectroscopy," *Angew. Chemie,* **55**, 6877–6881, 2016.
13. L. Luo, L. Men, Z. Y. Liu, Y. Mudryk, X. Zhao, Y. X. Yao, J. M. Park, R. Shinar, J. Shinar, K. M. Ho, I. E. Perakis, J. Vela, and J. G. Wang, "Ultrafast terahertz snapshots of excitonic Rydberg states and electronic coherence in an organometal halide perovskite," *Nature Commun.,* **8**, 15565, 2017.
14. M. T. Ruggiero, W. Zhang, A. D. Bond, D. M. Mittleman, and J. A. Zeitler, "Uncovering the connection between low-frequency dynamics and phase transformation phenomena in molecular solids," *Phys. Rev. Lett.,* **120**, 196002, 2018.
15. W. Zhang, J. Maul, D. Vulpe, P. Z. Moghadam, D. Fairen-Jimenez, D. M. Mittleman, J. A. Zeitler, A. Erba, and M. T. Ruggiero, "Probing the mechanochemistry of metal-organic frameworks with low-frequency vibrational spectroscopy," *J. Phys. Chem. C,* **122**, 27442–27450, 2018.
16. J. S. Jang, T.-I. Jeon, Y. J. Lee, J. H. Yoon, and Y. Lee, "Characterization of alpha-hydroquinone and beta-hydroquinone clathrates by THz time-domain spectroscopy," *Chem. Phys. Lett.,* **468**, 37–41, 2009.
17. E. S. Lee, K. W. Han, J. H. Yoon, and T.-I. Jeon, "Probing structural transition and guest dynamics of hydroquinone clathrates by temperature-dependent terahertz time-domain spectroscopy," *J. Phys. Chem. A,* **115**, 35–38, 2011.
18. J. P. Torré, R. Coupan, M. Chabod, E. Pere, S. Labat, A. Khoukh, R. Brown, J. M. Sotiropoulos, and H. Gornitzka, "CO_2-hydroquinone clathrate: Synthesis, purification, characterization and crystal structure," *Cryst. Growth Des.,* **16**, 5330–5338, 2016.
19. W. Zhang, D. Nickel, and D. Mittleman, "High-pressure cell for terahertz time-domain spectroscopy," *Opt. Express,* **25**, 2983–2993, 2017.
20. R. Dovesi, A. Erba, R. Orlando, C. M. Zicovich-Wilson, B. Civalleri, L. Maschio, M. Rérat, S. Casassa, J. Baima, S. Salustro, and B. Kirtman, "Quantum-mechanical condensed matter simulations with CRYSTAL," *WIREs Comput. Molec. Sci.,* **8**, e1360, 2018.
21. J. P. Perdew, K. Burke, and M. Ernzerhof, "Generalized gradient approximation made simple," *Phys. Rev. Lett.,* **77**, 3865–3868, 1996.
22. S. Grimme, J. Antony, S. Ehrlich, and H. Krieg, "A consistent and accurate *ab initio* parametrization of density functional dispersion correction (DFT-D) for the 94 elements H-Pu," *J. Chem. Phys.,* **132**, 154104, 2010.
23. A. Schäfer, H. Horn, and R. Ahlrichs, "Fully optimized contracted Gaussian basis sets for atoms Li to Kr," *J. Chem. Phys.,* **97**, 2571–2577, 1992.
24. M. Bouvet, B. Malézieux, and P. Herson, "A quinhydrone-type 2 : 1 acceptor-donor charge transfer complex obtained via a solvent-free reaction," *Chem. Commun.,* 1751-1753, 2006.
25. E. Eikeland, M. K. Thomsen, J. Overgaard, M. A. Spackman, and B. B. Iversen, "Intermolecular interaction energies in hydroquinone clathrates at high pressure," *Cryst. Growth Des.,* **17**, 3834–3846, 2017.
26. F. Pascale, C. M. Zicovich-Wilson, F. López Gejo, B. Ciuvalleri, R. Orlando, and R. Dovesi, "The calculation of the vibrational frequencies of crystalline compounds and its implementation in the CRYSTAL code," *J. Comp. Chem.,* **25**, 888–897, 2004.
27. C. M. Zicovich-Wilson, F. Pascale, C. Roetti, V. R. Saunders, R. Orlando, and R. Dovesi, "Calculation of the vibration frequencies of alpha-quartz: the effect of Hamiltonian and basis set," *J. Comp. Chem.,* **25**, 1873-1881, 2004.
28. Y. Noel, C. M. Zicovich-Wilson, B. Civalleri, P. D'Arco, and R. Dovesi, "Polarization properties of ZnO and BeO: An *ab initio* study through the Berry phase and Wannier functions approaches," *Phys. Rev. B,* **65**, 014111, 2001.
29. R. Dovesi, B. Kirtman, L. Maschio, J. Maul, F. Pascale, and M. Rérat, "Calculation of the infrared intensity of crystalline systems. A comparison of three strategies based on Berry phase, Wannier function, and coupled-perturbed Kohn–Sham methods," *J. Chem. Phys. C,* **123**, 8336–8346, 2019.

30. A. Erba, J. Maul, M. Ferrabone, P. Carbonnière, M. Rérat, and R. Dovesi, "Anharmonic vibrational states of solids from DFT calculations. Part I: Description of the potential energy surface," *J. Chem. Theory Comput.,* **15**, 3755–3765, 2019.
31. A. Erba, J. Maul, M. Ferrabone, R. Dovesi, M. Rérat, and P. Carbonnière, "Anharmonic vibrational states of solids from DFT calculations. Part II: Implementation of the VSCF and VCI methods," *J. Chem. Theory Comput.,* **15**, 3766–3777, 2019.
32. S. C. Wallwork and H. M. Powell, "The crystal structure of the a form of quinol," *J. Chem. Soc. Perkins Trans.,* **2**, 641–646, 1980.
33. S. Fan, M. T. Ruggiero, Z. Song, Z. Qian, and V. P. Wallace, "Correlation between saturated fatty acid chain-length and intermolecular forces determined with terahertz spectroscopy," *Chem. Commun.,* **55**, 3670–3673, 2019.
34. A. Galano and J. R. Alvarez-Idaboy, "A new approach to counterpoise correction to BSSE," *J. Comp. Chem.,* **27**, 1203–1210, 2006.